ISTITUTO NAZIONALE DI RICERCA METROLOGICA
Repository Istituzionale

Tuning ZnO Nanowire Dissolution by Electron Beam Modification of Surface Wetting Properties

(Article begins on next page)

20 March 2024

Tuning ZnO Nanowire Dissolution by Electron Beam Modification of Surface Wetting Properties

Gianluca Milano[†§], Luca D'Ortenzi[‡], Katarzyna Bejtka[§], Luisa Mandrile[¶], Andrea M. Giovannozzi[¶], Luca Boarino[‡], Candido F. Pirri[†§], Carlo Ricciardi[†] and Samuele Porro[†]*

[†]Department of Applied Science and Technology, Politecnico di Torino, C.so Duca degli Abruzzi 24, 10129 Torino, Italy.

[§]Center for Sustainable Future Technologies, Istituto Italiano di Tecnologia, C.so Trento 21, 10129 Torino, Italy.

[‡]Nanoscience and Materials Division, INRiM (Istituto Nazionale di Ricerca Metrologica), Strada delle Cacce 91, 10135 Torino, Italy.

[¶]Metrology for the quality of life division, INRiM (Istituto Nazionale di Ricerca Metrologica), Strada delle Cacce 91, 10135 Torino, Italy.

ABSTRACT

The ability of modifying the surface properties plays a crucial role in nanostructures where the high surface-to-volume ratio is often exploited for a various range of applications. In this work, the anisotropic dissolution of ZnO nanowires (NWs) in water was analysed and a reversible method for the modification of the surface wetting properties based on electron beam irradiation

was investigated. Using this approach, it was possible to selectively modify the wetting properties of single-crystalline ZnO NWs from hydrophilic to hydrophobic, preventing the degradation of these nanostructures when exposed to water. As deeply investigated by means of spectroscopic analyses, the switching mechanism of wettability was ascribed to the modification of organic compounds on the surface induced by electron beam irradiation. In particular, it was observed that the main effect of electron beam irradiation was to induce decomposition of hydrocarbons on the NW surface, with the consequent creation of radicals and reorganization of organic chains. In addition, we show that electron beam irradiation promotes the interaction of these nanostructures with an organic polymer (PMMA). The reversibility of the surface modifications was obtained by means of an oxygen plasma treatment that restored the initial hydrophilic properties of the nanostructures. The same principle could be exploited for controlling dissolution and avoiding corrosion of other nanostructures and films at the nanoscale.

INTRODUCTION

Semiconductor nanostructured materials have recently attracted enormous attention due to the high surface-to-volume ratio and distinctive charge transport properties[1]. In addition, nanowire-based electronics is promising as a result of the extreme scalability, beyond the limits of conventional lithography. Among nanostructured materials, ZnO nanowires (NWs) are widely studied because of their peculiar photonic, plasmonic, mechanical, and electronic properties.[2–5] ZnO nanostructures can be grown independently or on different substrates, using both vapor phase or solution phase synthesis and allowing a large-scale and low-cost production.[6,7] All these characteristics make ZnO NWs a multifunctional material suitable for a wide range of applications and particularly promising for being used as building block for the realization of a

new class of electronic devices, such as field effect transistors,[8] resistive switching devices[9–11] and sensors.[12,13] Owing to biocompatibility and biosafety of ZnO, structures of this material are also considered good platforms for biomedical applications.[14,15]

Despite the wide range of applications, chemical stability and solubility of these nanostructures can have a strong impact on biological purposes as well as electronic devices reliability. Even though ZnO nanostructures are generally considered chemically stable, degradation and corrosion of ZnO was observed in atmospheric conditions under prolonged exposure to environmental moisture or high relative humidity, after interaction with water and after hydrothermal treatments.[16–20] In particular, it was observed that ZnO corrosion strongly depends on humidity, CO_2 concentration and substrates.[16] Indeed, ZnO can interact with water and form zinc hydroxide and subsequently this hydrated layer can react with CO_2 to form zinc carbonates on the surface that can strongly affect the electrical and optical properties of ZnO NWs.[17] On the other hand, ZnO corrosion and solubility play a key role for enhancing biodegradability and biocompatibility. Zhou et al.[20] pointed out that ZnO dissolution can occur in biofluids and in both acidic and basic conditions. Being Zn^{2+} ions indispensable trace elements for human body, dissolution products of ZnO NWs can be absorbed becoming part of nutrition. ZnO nanostructures are thus good candidates for becoming "deliver and dissolve" platforms for cancer imaging and therapy and for drug targeting, if dissolution rate and delivery could be controlled.[15]

In this scenario, understanding and controlling the corrosion and degradation process of ZnO nanostructures becomes of great interest in many research fields. In this work, the dissolution process of ZnO NWs in water is investigated in details and an approach for modifying the wetting properties of the ZnO nanostructure surfaces is analysed. As discussed in previous

works, electron beam irradiation can be used for modifying surface wetting properties of thin films and nanomaterial powders,[21–26] for surface functionalization[27] and for micromachining[28–30]. In our work, the effect of electron beam irradiation on ZnO NWs was discussed and deeply investigated by means of spectroscopic techniques. In particular, we show that this surface treatment can modify the NW wetting properties overcoming water vulnerability. By using this approach, it was possible to modify the surface properties at the nanoscale in a single selected NW. Moreover, full reversibility of the surface modifications was achieved by treating the e-beam exposed NWs with an O_2 plasma.

EXPERIMENTAL SECTION

Synthesis

The ZnO NWs synthesis was performed in a horizontal tubular furnace by Low Pressure Chemical Vapor Deposition (LP-CVD), as previously reported.[9] A substrate of Pt (100 nm)/Ta (20 nm) realized by sputtering on a SiO_2(190 nm)/Si wafer was used as a catalyst and placed in a quartz tube on an alumina boat, with a Zn foil (purity 99.99%) that was used as the Zn source. The process was performed at 650°C, fluxing 300 sccm of Ar (carrier gas) and 200 sccm of O_2 (precursor). During the deposition process, the pressure was 1.6 mTorr.

Characterization

As grown ZnO nanostructures were characterized by field emission scanning electron microscopy (FE-SEM; Zeiss Merlin). Elemental analysis was conducted in the FE-SEM equipped with an EDX Oxford X-act with a 10^2 mm SDD detector, using electrons accelerated at 15 kV. Structural characterization was performed by X-ray diffraction (XRD) in Bragg–Brentano theta-2 theta configuration. Transmission Electron Microscopy (TEM) was performed with a FEI

Tecnai F20ST equipped with a field emission gun (FEG) operating at 200 kV. The TEM sample was prepared by transferring the ZnO NWs from the growth substrate onto the TEM grid with the use of a mounted hair. Chemical composition of the ZnO NWs surface was investigated by means of X-ray photoelectron spectroscopy (XPS), using a Kα source with energy of 1486.6 eV. An Ar ion gun (sputtering rate ~ 300 Å/min) was used to remove ZnO from the surface and to investigate the bulk chemical composition.

Electron beam irradiation and O_2 plasma treatment

Vertically aligned NWs were mechanically removed from the growth substrate using a Cu wire and then deposited on a SiO_2 substrate. In this way, it was possible to avoid direct exposure of NWs to any solvent during this step. Tests of surface modification induced by electron beam irradiation of dispersed NWs were performed in vacuum (~ 10^{-5} mbar) at room temperature inside a scanning electron microscopy chamber (SEM; FEI Inspect F™), with electrons accelerated at 30 kV, using a working distance of 10 mm. Electron irradiation of NWs was performed scanning the beam with the video rate to reduce sample heating.[31] Oxygen plasma treatment was performed in a Bdiscom Plasma Matrix, using 40 W of power for 60 s at a pressure of ~ 3 x 10^{-2} mbar. The dissolution and corrosion tests on treated and untreated isolated NWs were performed by means of SEM and using markers as references. TEM characterization of corroded NWs was performed after inserting the TEM grid with ZnO NWs in deionized water for 60 minutes. Modifications of ZnO NWs after treatments were investigated considering ZnO NW arrays, irradiating by electron beam a selected area of the sample. Using markers as references, the same area of the sample was investigated by Raman and FT-IR spectroscopy before and after the treatments. Raman spectroscopy was performed using a confocal Thermo Fisher Scientific DXR Raman microscope system equipped with an excitation laser source at 532

nm, a 100x microscope objective and a full range grating (acquisition range: 50-3500 cm^{-1}) with a spectral resolution of 5 cm^{-1}. The laser power was limited to 2 mW to avoid thermal degradation of the sample and the exposure time for each spectrum was set to 1 second per 20 scans in total. Raman mapping was performed on an area of 10 by 100 μm with a step-size of 2 μm. Infrared spectroscopy measurements were performed in reflectance mode with a iN10 FT-IR microscope (Thermo Fisher Scientific) equipped with a liquid nitrogen cooled MCT detector, a 15x microscope objective and a spot size of 100 μm x 100 μm. Each spectrum was collected with 64 scans in a spectral range 650 - 4000 cm^{-1} with a resolution of 4 cm^{-1}. The background was collected with the same collection parameters on a clean and flat gold surface. The FTIR peaks were fitted using a multiple fit peak function present in Omnic Software 9.3 using a mixed Lorentzian/Gaussian function. The number of fitted peaks was declared before the calculation.

RESULTS AND DISCUSSION

Growth and characterization of NWs

As a consequence of the LP-CVD process, high density and vertically aligned NWs were grown.[9,32] The morphological characterization of NWs by SEM is reported in Figure 1 a). The single crystal and hexagonal shaped NWs have an average length of ~ 1.6 μm and an average diameter of ~ 100 nm (aspect ratio of ~ 15) with a density of ~10 μm^{-2}.

The characterization of the NW array by means of EDX (Figure 1 b)) confirms the presence of Zn and O while the presence of Pt and Si is linked to the underlying growth substrate. Even if this technique is not suitable to investigate traces of elements and small contamination (especially light elements on the surface), it is possible to exclude the presence of high

contaminations after the growth process, except for the presence of carbon species on the surface due to sample exposure to atmospheric conditions. XRD characterization was performed in order to examine the crystal structure of the grown nanostructures. XRD pattern (Figure 1 c)) of vertically aligned NWs reveals a well match with the wurtzite crystal structure of ZnO (w-ZnO) with P6$_3$*mc* symmetry. A strong peak located at 2θ equal to 34.53° dominate the pattern and is a consequence of the diffraction of the (002) plane of w-ZnO. A peak relative to the [101] orientation was observed at 2θ equal to 36.37° while peak located at 63.06° can be associated to the [103] orientation. In addition, peaks of Pt and Si in the XRD pattern are linked to the substrate. A comparison between peak intensity in ZnO NW XRD pattern with pattern from ZnO powder (from standard data file JCPDS No. 89-0511) revealed that NWs are highly oriented in the [002] direction, as a consequence of the growth along the c-axis direction. Wurtzite ZnO NWs grown along the c-axis direction are characterized by a (002) polar surface (top of NW) while other surfaces are non-polar. In order to investigate the chemical stability of these nanostructures, ZnO NWs were exposed to normal laboratory environment for about 1 year. After this period, the NW surface was investigated by TEM. Differently from what reported by Pan et al.,[16] our LP-CVD grown NWs do not exhibit significant degradation due to the exposure to normal ambient environment conditions. In particular, high-resolution TEM measurements confirmed the high crystallinity with perfect lattice structure of NW and exclude the presence of an amorphous $ZnCO_3$ thin layer on the surface of LP-CVD grown NWs, as reported in Figure 1 d).
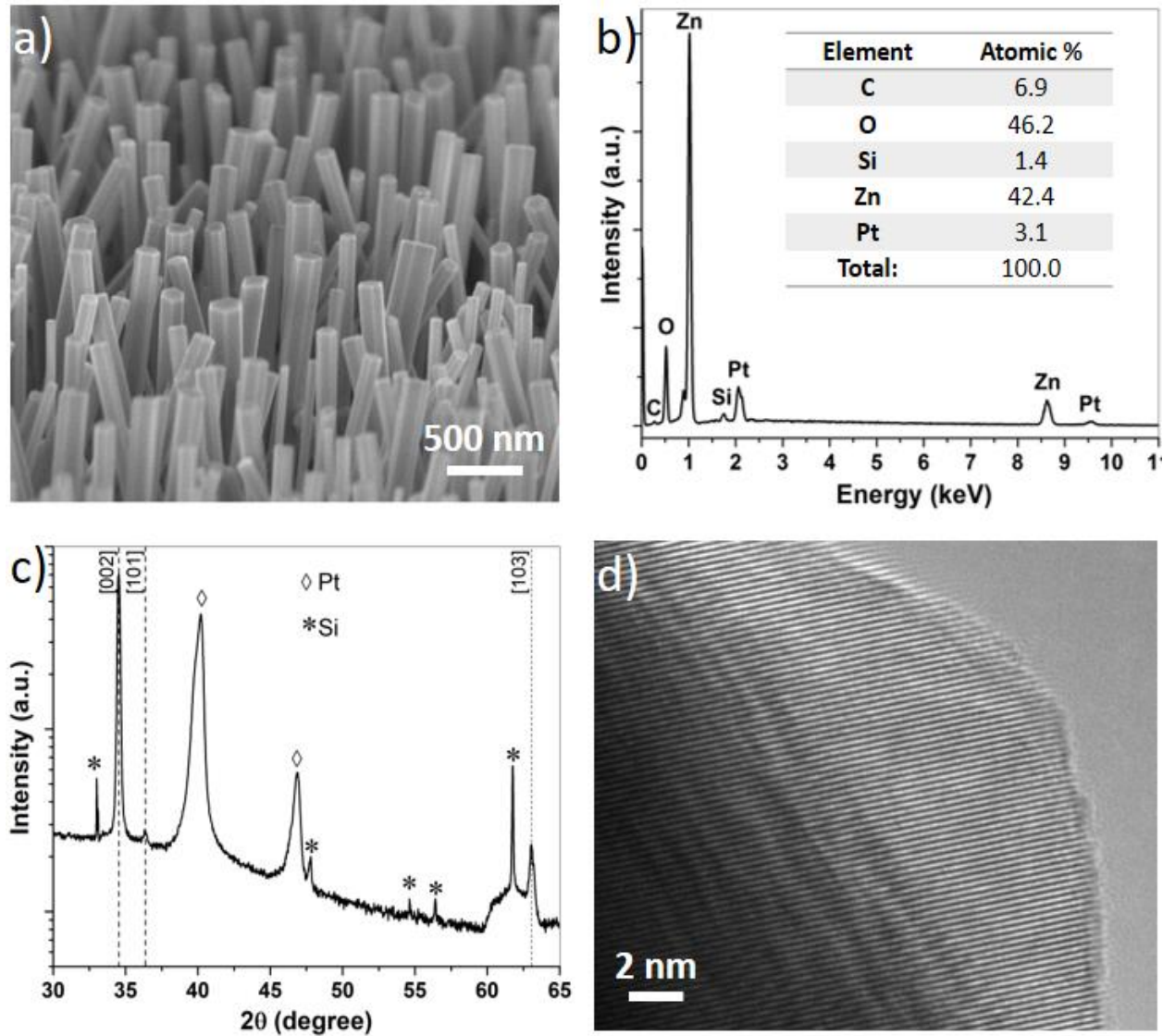
Figure 1. a) Tilted FE-SEM image of as grown vertically aligned and hexagonal shaped ZnO NWs; b) EDX spectra and c) XRD pattern acquired on vertically aligned NWs after the growth process (intensity is in log scale); d) high resolution TEM image of the ZnO NW surface after ~ 1 year of exposure to ambient environment.

Wettability and dissolution of ZnO NWs in H₂O

ZnO NWs dispersed on SiO₂ substrate were immersed in deionized water (pH ~ 6.7-6.9, conductivity ~ 150 μS/cm) in order to investigate the dissolution process of a single NW. As a consequence of the interaction with H₂O, the surface of NWs was highly corroded, with the consequent diameter reduction and mass loss. The degradation of ZnO NWs in water as a function of exposure time is presented in Figure 2. Even if the dissolution rate is slightly
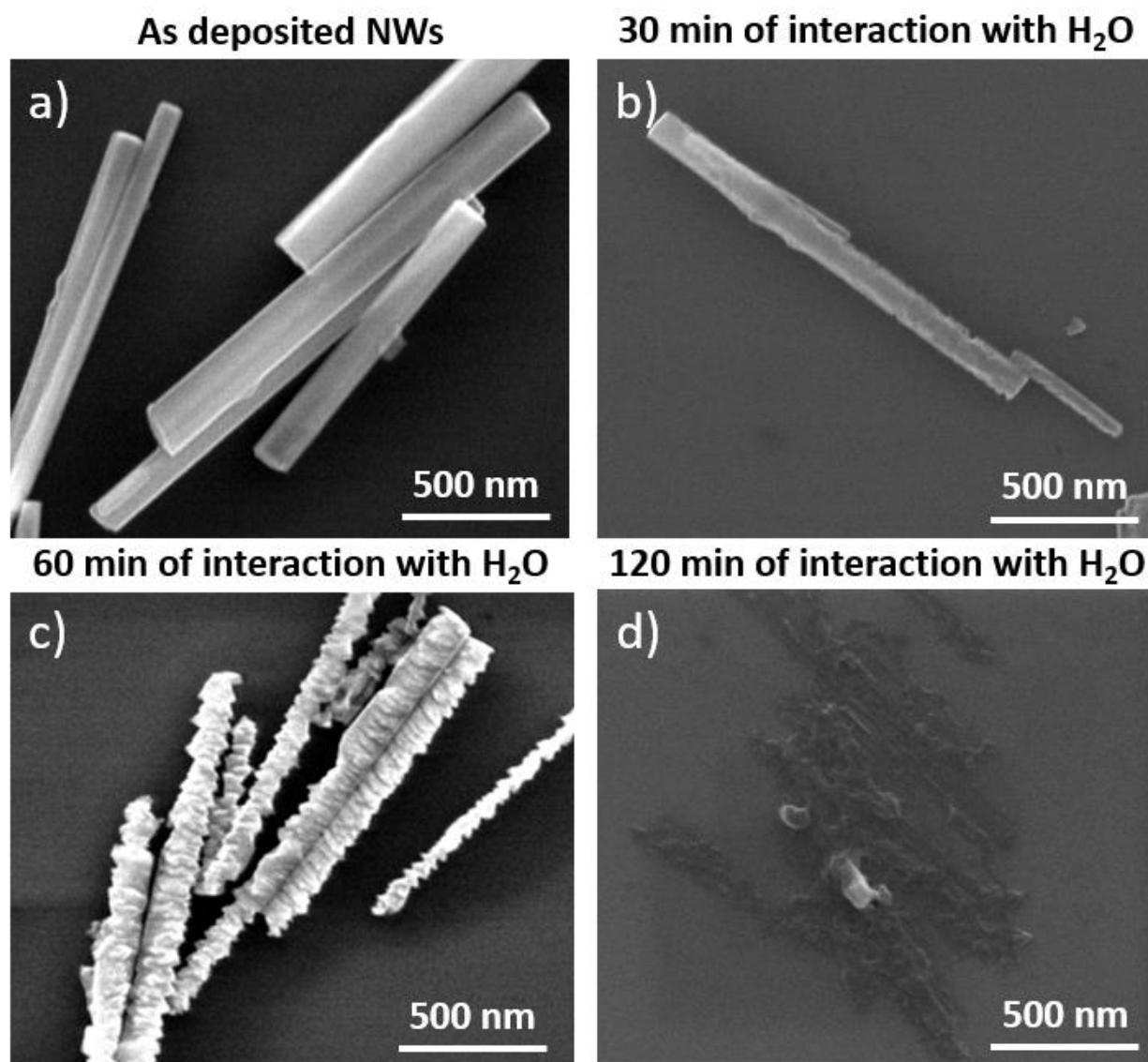
Figure 2. FE-SEM images of ZnO NWs deposited on SiO₂ substrate before and after the interaction with deionized water; a) NWs before interaction, b) after 30 min of interaction, c) after 60 min of interaction and d) after 120 min of interaction.

different from NW to NW, after 30 min of interaction the surface resulted to be wrinkled and slightly corroded (Figure 2 b)). The corrosion of the surface becomes more evident after 60 min of water exposure, and NWs resulted to be characterized by an irregular surface with increased roughness (Figure 2 c)). After 120 min of interaction with H_2O, NWs were almost completely dissolved and only some residues of ZnO were present on the underlying substrate (Figure 2 d)).

The dissolution process of ZnO NWs in water can be attributed to the chemical dissociation:[33,34]

$$ZnO(s) + H_2O \xrightarrow{K_{sp}} Zn^{2+} + 2OH^- \qquad (1)$$
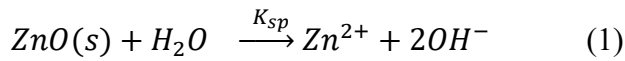
where K_{sp} represents the solubility product. The wetting properties of NW surfaces are strongly influenced by defects.[35,36] In order to investigate the peculiar properties of the ZnO NW surface, XPS measurements were performed on the ZnO NW array surface and after 10 min of Ar^+ sputter etching (bulk). Results are shown in Figure 3. XPS spectra confirmed a high chemical purity of ZnO NWs, revealing the presence of Zn and O peaks. However, carbon contaminations were observed on NW surfaces and disappeared after surface sputtering, as shown in Figure 3 a) and b), revealing that these contaminations are the consequence of sample exposure to atmosphere (details and high-resolution spectra of C are reported in Supplementary Information S1). A more detailed analysis can be performed considering high-resolution XPS spectra of O and Zn, where peaks were fitted using a Gaussian-Lorentzian function after Shirley's background subtraction. O 1s high-resolution spectra of ZnO NW surface and after sputtering are presented in Figure 3 c) and d), respectively. In both cases it was observed that raw data can be consistently fitted by three components, reflecting different oxygen environments. The dominant component (O_a), located at 530.3 eV for the surface and at 530.5 eV for bulk, can be attributed to O^{2-} ions surrounded by Zn^{2+} ions in the hexagonal wurtzite structure (Zn-O bond).[37] The binding

energy peak located at 531.6 eV for the surface and 531.7 for bulk (O_b) can be assigned to O^{2-} ions in oxygen-deficient regions.[38] Instead, the third component (O_c) located at 532.2 eV for the surface and 532.6 eV for bulk are ascribable to the presence of hydroxyl groups.
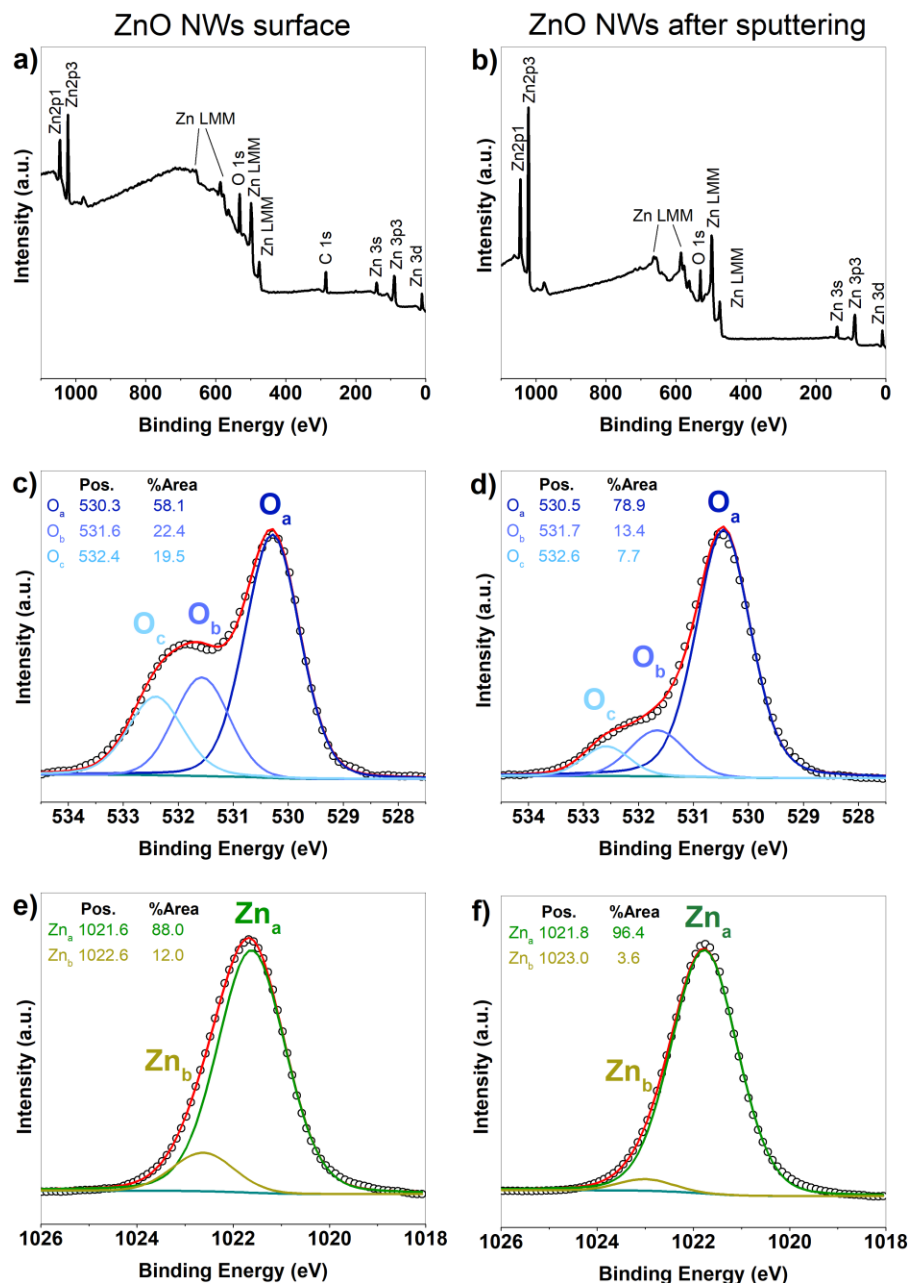
Figure 3. Survey spectra of ZnO NW array after the growth process a) on the surface and b) after 10 min of sputtering (bulk). High-resolution spectra of O 1s core level c) on the surface and d) bulk. High-resolution spectra of Zn2p$_{3/2}$ level e) on the surface and f) bulk. Peaks were fitted with Gaussian-Lorentzian functions, after Shirley's background subtraction. The cumulative fit peak is reported in red while circles are raw data.

The shift towards higher binding energies of this component is due to the higher electronegativity of hydrogen, resulting in less negatively charged oxygen atoms.[39] High-resolution spectra of Zn $2p_{3/2}$ are presented in Figure 3 e) and f) for the surface and for bulk, respectively. In both cases the asymmetric peak can be interpolated with two components. The main component, located at 1021.6 eV for the surface and 1021.8 eV for bulk, can be attributed to the oxide form of Zn (ZnO) while the high energy shoulders (located at 1022.6 eV for the surface and 1023.0 eV for bulk) are related to a hydrated layer on the ZnO surface (zinc hydroxide).[40] A high-energy shoulder was also observed considering the Zn $2p_{1/2}$ peak that is located at 1044.7 eV in case of surface and 1044.9 eV in case of bulk (details in Supplementary Information S2). In both cases, the peak separation of 23.1 eV between Zn $2p_{1/2}$ and $2p_{3/2}$ is in good agreement with the standard reference value for ZnO.[41] A comparison of high-resolution XPS spectra before and after sputtering revealed that the surface is more defective respect to bulk. Indeed, the oxygen vacancies as well as the hydroxyl groups concentration decreased in bulk, as confirmed by the decreasing in intensity of O_b and O_c components after sputtering. This evidence was supported also by the reduction of Zn_b component respect to Zn_a after Ar^+ sputtering.

Surface defectiveness can facilitate the dissolution of ZnO NWs in water. Indeed, surface defects can be considered as active sites for water dissociation and adsorption.[42] Ali et Winterer[43] reported that doubly charged oxygen vacancies ($V_O^{\bullet\bullet}$), that are thermodynamically favoured in ZnO, can be active sites for dissociative chemisorption on the ZnO surface through the generation of hydroxyl groups (using the Kröger-Vink notation):

$$V_O^{\bullet\bullet} + O_O{}^x + H_2O(g) \rightarrow OH_O{}^{\bullet} + OH_O{}^{\bullet} \tag{2}$$

Furtheremore, hydroxyl groups already present on the surface after ambient exposure can lead to

higher probability of H_2O dissociation, facilitating the water wetting and increasing the hydrophilicity of these nanostructures.[36] Thus, the ZnO NWs dissolution is facilitated by oxygen vacancies and hydroxyl groups on the surface. It was also observed that the dissolution of NWs was not isotropic and the hexagonal shape was not conserved after corrosion, as a consequence of the more reactive edges. Furthermore, while the diameter is drammatically reduced, the length of NWs was not affected by the corrosion before the complete dissolution of the NW. This indicates that the polar (002) surface of NW is less sensible to the corrosion process respect to other non-polar surfaces (as can be seen in Figure 4 a) and b)). Indeed, the polar surface remained smooth at all its length. The stability of the (002) planes in ZnO is probably influenced by surface reconstruction effects. Indeed, surface reconstruction in non-polar surfaces involves only the tilt of cations-anions dimers while a massive surface reconstruction or faceting can occur in polar surfaces, with the presence of vacancies, adsorbates and impurities on the surface layer.[36] For these reasons the wetting properties of the (002) surfaces can be strongly modified. Moreover, after the interaction with water, sharp edges were observed on the lateral surfaces of NWs, as can be clearly seen in TEM, STEM and FE-SEM images (Figure 4 a), b) and c)). These crystallographic planes parallel to growth direction, which are symmetrical (100) non-polar facets, were previously smooth walls. A more detailed information can be obtained from analysis performed by high-resolution TEM (HRTEM), as can be seen from Figure 4 d), where the high magnification of a sharp edge is shown. The clear lattice fringes observed indicate good crystal quality and the c-axis growth direction was indicated by lattice fringes with d-spacing of 0.52 nm. The angle measurement of edges respect to the [002] direction revealed an angle of ~ 62°, that is consistent with the presence of the (101) crystallographic orientation (according to JCPDS No. 89-0511 the expected value for the angle between (101) and (002) planes is 61.6°). This

means that non-polar (100) surfaces on the NW are more sensitive to water corrosion respect to (101) and (002) surfaces. It is important to notice that anisotropic dissolution was observed by Qi et al.[44] also in case of ZnO wires after interaction with HCl solution. In addition, HRTEM images revealed that amorphization of the surface did not occur after the interaction with water and excluded the formation of zinc carbonates arising from carbon material due to atmosphere exposure (additional TEM and HR-TEM images are reported in Supplementary Information S3).
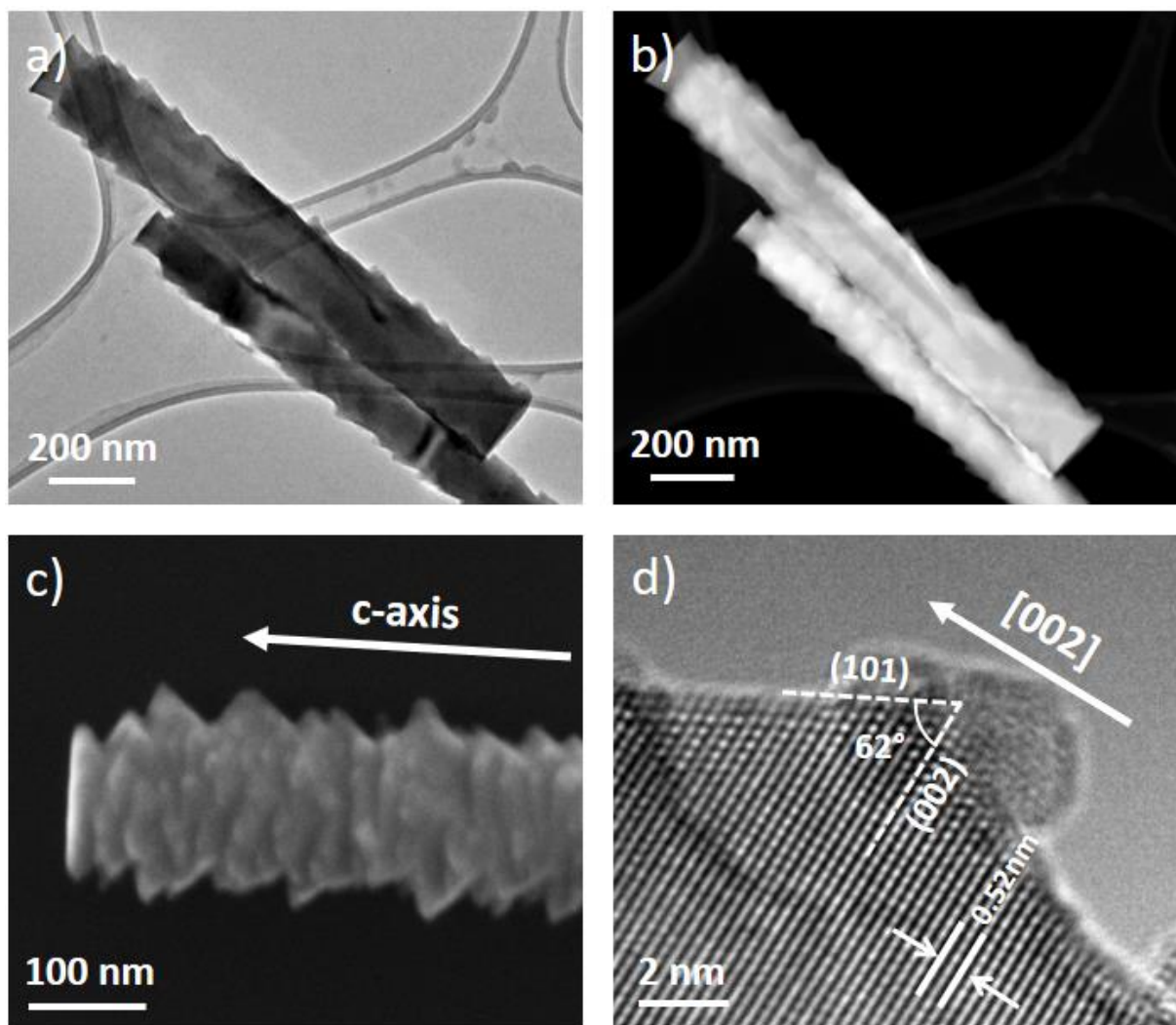
Figure 4. a) Bright-field TEM image, b) STEM image and c) FE-SEM image of a ZnO NW after 60 min of exposure to deionized water; d) HR-TEM image showing details of the anisotropic corrosion of the ZnO NW.

14

Z. Pan et al.[16] pointed out that the chemical stability of ZnO nanostructures can be influeced by the supporting substrate and the processing history. Indeed, under ambient conditions the oxide substrate is hydrated because water vapors can be absorbed dissociatively on the oxide surface, forming active sites such as ≡MOH, ≡M-O(H)-M≡ etc..[45] In order to understand if the degradation of ZnO NWs is facilitated by the SiO_2 substrate, degradation tests were performed depositing NWs on different substrates. Our results showed that the degradation process of ZnO NWs is not substrate dependent and, after 60 min of interaction with deionized H_2O, surface corrosion was observed also on NWs deposited on Al_2O_3 and Si_3N_4 substrates (details of ZnO NW degradation on Al_2O_3 and Si_3N_4 substrates are reported in Supplementary Information S4).

Modification of wettability properties by electron beam irradiation

Our observations showed that it was possible to modify the wetting properties of ZnO NWs by electron beam irradiation, avoiding the dissolution of ZnO NWs in water. In order to explain this behaviour, it is necessary to take into account a modification of the surface energy after the electron irradiation that can be responsible for the transition between the hydrophilicity (high surface energy) and the hydrophobicity (low surface energy) of the ZnO NW surfaces. Thus, the reduced affinity of ZnO NW surfaces with water can prevent the ionic dissolution of Zn^{2+} ions. Selected single ZnO NWs (markers were used as position references) were irradiated by electron beam fixing the values of exposure time at 120 s and magnification at 120000×, which correspond to an exposed area of 5.36 μm^2. The measured beam current was 116 pA and, using these experimental conditions, the electron dose was calculated to be Q=0.26 C cm^{-2}. Afterwards, exposed NWs were immersed into deionized H_2O for 60 min together with a control sample of untreated ZnO NWs. As reported in Figure 5, the e-beam exposed NWs did not show

any degradation and dissolution of the surface after water interaction and conserved the initial hexagonal shape while corrosion of the surface was observed in the untreated control sample. It is worth noticing that, exposing only selected areas to electron beam irradiation, it is possible to selectively modify the wetting properties of a single ZnO NW (details of selective tuning of the wetting properties is reported in Supplementary Information S5).
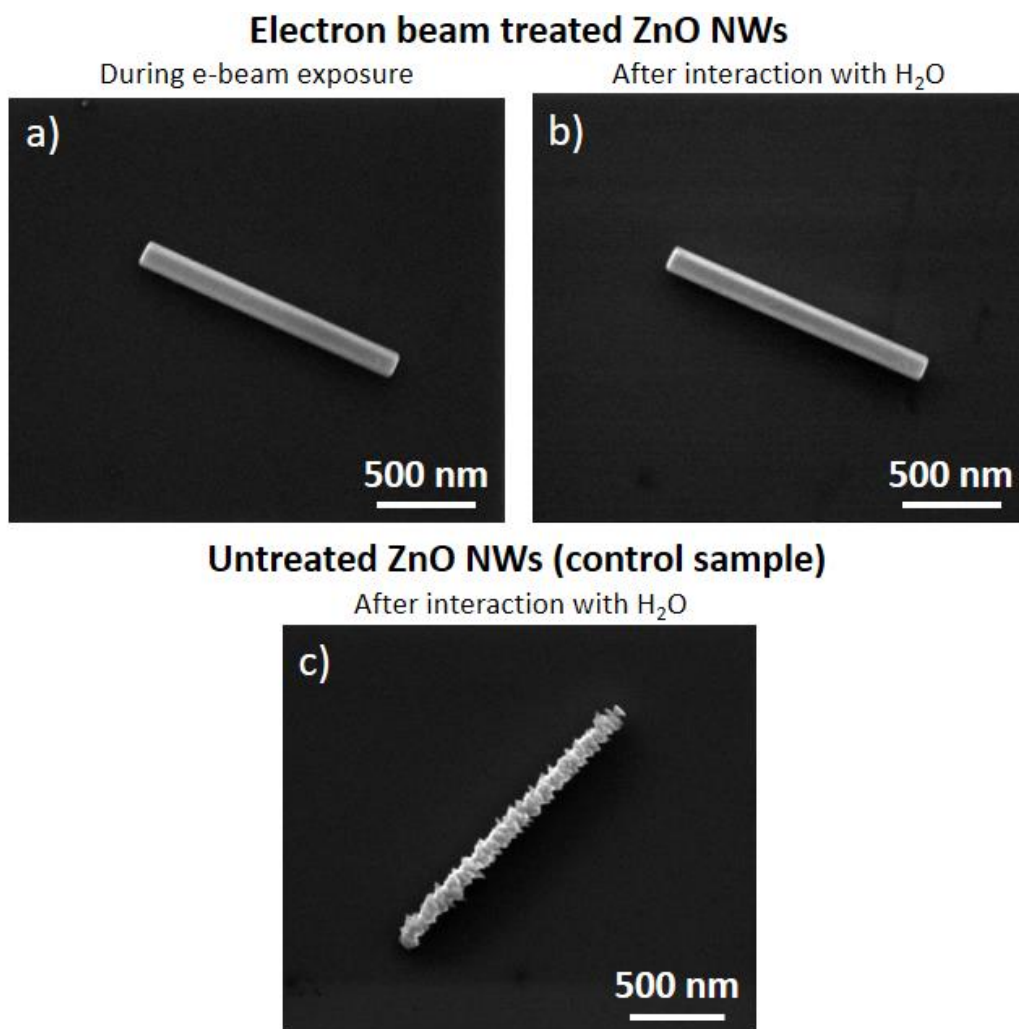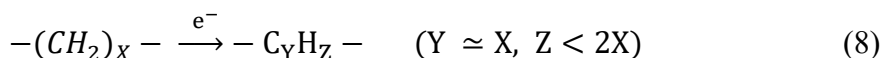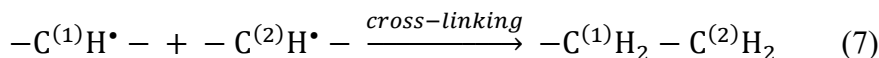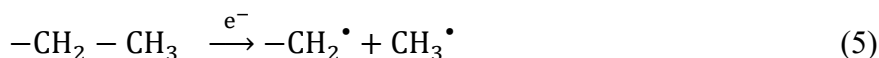

Figure 5. FE-SEM image of the same ZnO NW on a SiO$_2$ substrate a) during e-beam exposure and b) after 60 min of interaction with deionized H$_2$O; c) SEM image of an untreated ZnO NW after 60 min of interaction with deionized H$_2$O (control sample).

Mechanism of modification of the wettability properties

In order to understand the change of the wetting behaviour of these nanostructures, several aspects have to be considered. As discussed in previous works by Aronov et al.[21–23] and Torchinsky et al.[24], the irradiation of solid surfaces by electrons can be responsible for defect generation, electrical charging and chemical modifications. All these effects can have a strong influence on the surface energy and wettability properties of solid materials. However, the electron irradiation energy used in our experiment (E_e= 30 kV) was less than one order of magnitude than the energy required for atomic displacement and defects generation in wurtzite ZnO.[46] For this reason, the generation of surface defects induced by the electron beam irradiation is improbable. This hypothesis was further corroborated by our TEM analysis that do not evidenced any defect generation even when NWs were irradiated by electrons at 200kV, as previously reported in Figure 1 d). Even if for low doses of electron irradiation the electron induced charging governs the wettability variation, for high doses irradiation ($Q > 1.5\ \mu C\ cm^{-2}$) chemical contaminations can affect the surface properties, as previously discussed by Aronov and Rosenman.[22] It is worth noticing that, in our experiment, the sample exposure to electron beam implies fairly high electron doses ($Q \sim 0.26\ C\ cm^{-2}$). In our case, organic compounds are unavoidably present on the NW surface as a consequence of atmospheric exposure before being exposed to electron beam irradiaton in the SEM chamber, as previously discussed by EDX and XPS measurements. The main components of organic compounds are hydrocarbons. When these species on the NW surface are irradiated with electrons, complex sequences of radical reactions can occur with the consequent reorganization and decomposition of the hydrocarbon chains. According to Seshadri et al.,[47] the main reactions can be summarized in this fashion:

$$-CH_3 \xrightarrow{\ e^-\ } -CH_2^{\bullet} + H^{\bullet} \qquad\qquad\qquad (3)$$

$$-CH_2 - \xrightarrow{e^-} -CH^{\bullet} - +H^{\bullet} \qquad (4)$$

$$-CH_2 - CH_3 \xrightarrow{e^-} -CH_2^{\bullet} + CH_3^{\bullet} \qquad (5)$$

$$-CH_2 - CH_2 - \xrightarrow{e^-} -CH_2^{\bullet} + {}^{\bullet}CH_2 - \qquad (6)$$

$$-C^{(1)}H^{\bullet} - + -C^{(2)}H^{\bullet} - \xrightarrow{cross-linking} -C^{(1)}H_2 - C^{(2)}H_2 \qquad (7)$$

$$-(CH_2)_X - \xrightarrow{e^-} -C_YH_Z - \qquad (Y \simeq X, \ Z < 2X) \qquad (8)$$

Reactions from (3) to (6) refer to the C-H and C-C bond scission as a consequence of electron irradiation, with the consequent creation of free radicals. After being created, radicals can reorganize by interchain cross-linking processes as described in reaction (7). As a consequence of preferential loss of H atoms relative to C atoms during e-beam irradiation, the formation of a carbonaceous material is possible, as described by reaction (8). This is a consequence of reorganization of atoms in molecular species such as H_2 and CH_4 that are lost to the environment. Even if electron beam irradiation is performed in vacuum conditions, radicals can be created not only by hydrocarbons that are already present on the NW surface after the previous environmental exposure, but also coming from residual gas atmosphere in the SEM chamber, as discussed in previous works.[48,49] This hypothesis is corroborated by XPS measurements performed after electron beam irradiation that showed an increasing C content on the sample and exclude the presence of other contaminants (details in Supplementary Information S6). The hydrocarbon radicals created by electron beam are highly reactive, and can subsequently be bounded to the NW surface, creating an electron-deposited CH-rich layer. As previously discussed by Torchinsky et al. [24,25] in case of diamond and ZnO powders, an electron-deposited CH-rich layer can modify the surface wettability because it possesses hydrophobic and

oleophilic properties. The reaction of incident electrons with hydrocarbons can thus be exploited in our case to tune the wettability of the NW surface from hydrophilic to hydrophobic, avoiding the ZnO NWs dissolution in H_2O. Indeed, the electron deposited CH layer on the ZnO NW surface acts as a protective layer that decreases the chemical etching rate, as previously observed by Sabayev et al.[26] in case of electron-irradiated Ga-doped ZnO films exposed to oxalic acid ($C_2H_2O_4$) and sodium hydroxide (NaOH) etchants.

Our observations showed that the surface modification was reversible. Indeed, with an oxygen plasma (40 W, 60 s) it was possible to remove the alkyl groups from the NWs surface, restoring the intrinsic hydrophilic properties of ZnO NWs. When the hydrophilicity is restored, dissolution of NWs in water was observed again (see Supplementary Information S7). The schematic representation of the reversible tuning of surface wetting properties of ZnO NWs is presented in Figure 6.
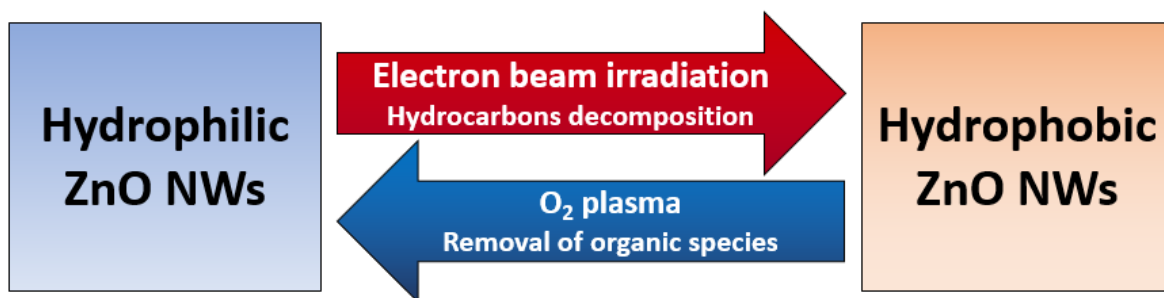
Figure 6. Schematic representation of the reversible tuning of surface wetting properties of ZnO NWs by electron beam irradiation that induces hydrocarbons decomposition, and O_2 plasma treatment that removes organic species from the NW surface.

In order to understand the mechanism of tuning the surface properties, modifications were deeply investigated by means of Raman and FT-IR spectroscopy by considering ZnO NW arrays. An area of $5.4 \cdot 10^4$ μm^2 of ZnO NW array was selected by means of reference markers and then

exposed to electron beam with a dose of Q= 0.066 C cm^{-2}. Afterwards the sample was treated with an oxygen plasma (40 W, 60 s). Raman and FT-IR measurements were performed at each step to investigate the surface modifications in the same selected area. The Raman spectrum of untreated ZnO NWs is reported in Figure 7 and showed the typical features of a wurtzite ZnO (w-ZnO).[50] The spectra are dominated by two narrow and intense modes that are associated to the E$_2$ symmetry. The low frequency E$_2$ peak can be identified at 100 cm^{-1} while the high-frequency E$_2$ peak is located at 436 cm^{-1}. These two non-polar modes involve mainly the motion
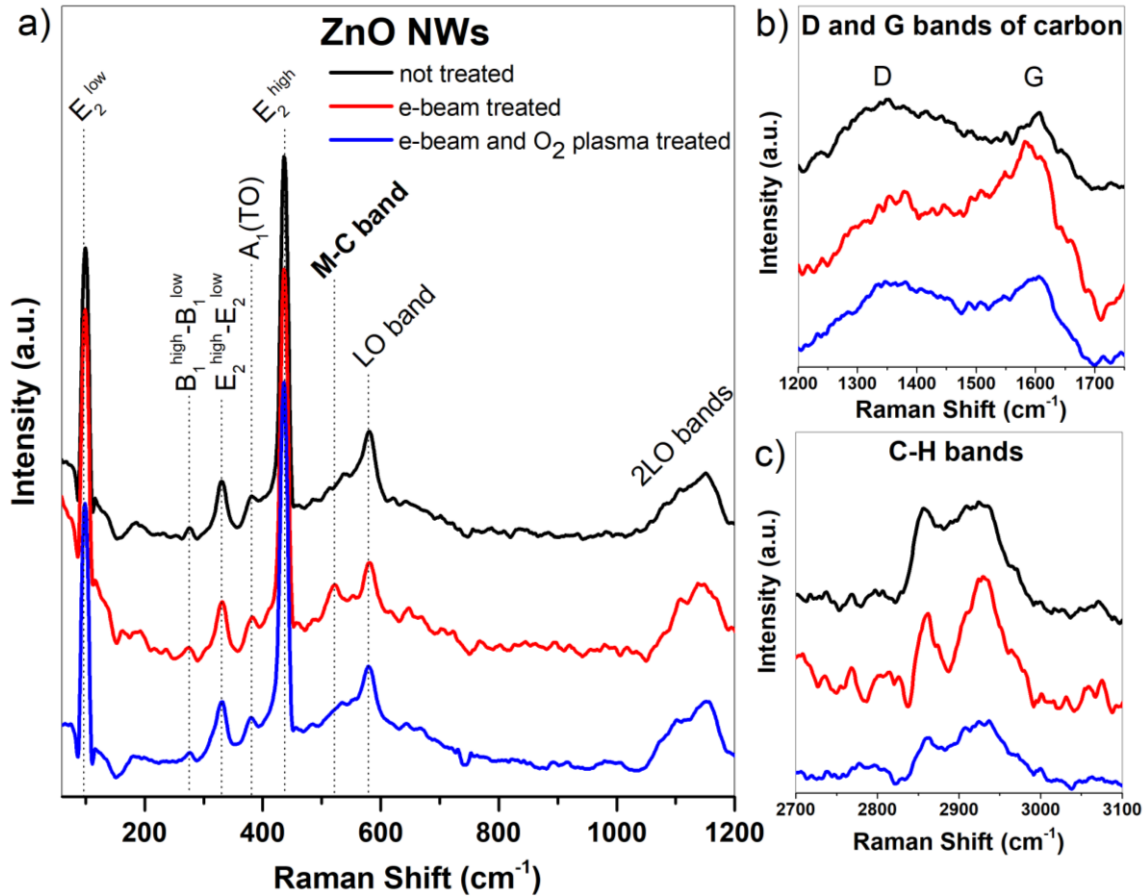
Figure 7. Raman spectra acquired on the same area of as grown ZnO NWs (black line), after the electron beam treatment (red line) and after the O$_2$ plasma treatment (blue line); a) the ZnO bands region, b) the carbon region and c) the CH bands region; all spectra are normalized on the E$_2$(high) peak of ZnO after background subtraction and are the result of at least 3 average spectra in different regions of the sample.

of Zn and O sublattices, respectively. Furthermore, oxygen dominated polar modes with A_1 and E_1 symmetries can be observed in the spectra. As a consequence of splitting of these modes into LO and TO modes, four peaks should be present in the spectra. A peak at 381 cm^{-1} can be associated with the A_1(TO) mode while the E_1(TO) mode (located at about 410 cm^{-1}) cannot be distinguished from the high frequency E_2 peak. An LO band can be identified at 581 cm^{-1} and it is associated to A_1(LO) and E_1(LO) modes with close wavenumbers. This broad band is usually correlated to the presence of intrinsic defects such as zinc interstitial and oxygen vacancies[51] while the asymmetry of this band can be attributed to silent modes of w-ZnO with B_1 symmetry allowed by the breakdown of translational crystal symmetry due to the presence of defects.[52] In addition, second order peaks can be identified in Raman spectra. Indeed, peaks at 278 cm^{-1} and 330 cm^{-1} can be associated to B_1^{high}-B_1^{low} and E_2^{high}-E_2^{low} difference modes, respectively. Furthermore, 2LO scattering processes with A_1 symmetry are responsible for the observation of two broad bands in the 1000-1200 cm^{-1} range. Typical features of carbonaceous materials are also present in as-grown ZnO NW Raman spectra in the range 1200-1800.[53] Indeed, it is possible to observe the graphitic G band located at $\sim$ 1600 cm^{-1} that arise from the stretching of C-C sp^2 bonds and the D band (defect-induced mode) located at $\sim$ 1350 cm^{-1} that is present in poorly ordered carbon species. The presence of carbon bands in the Raman spectra is due to residues of organic contaminants on the surface as a consequence of the ambient exposure. Additional bands associated to organic species can be observed in the 2800-3000 cm^{-1} range where bands can be assigned to C-H$_x$ stretching.[54] This broad bands are linked to symmetric and asymmetric stretching of CH$_2$ and CH$_3$ groups. After the electron beam irradiation, some spectral modifications were observed, especially in the amorphous carbon and C-H stretching regions. Indeed, an intensity growth of the G band (I_G) of amorphous carbon was registered. The

consequent decrease in I_D/I_G ratio after electron irradiation suggests an ongoing carbonization process of organic species. This is a consequence of the increased C-C sp^2 content in carbonized products.[55] The degradation, and more precisely, the carbonization of the organic material on the NW surface was due to the incident electron beam energy, as described by reaction (8). After the e-beam irradiation some changes were also observed in the C-H stretching region where two more resolved peaks at about 2860 cm^{-1} and 2925 cm^{-1} show up. These two modes can be assigned to CH_2 symmetric and asymmetric stretching, respectively. The transformation of the C-H broad band into two resolved peaks can be attributed to the band width decreasing of the symmetric CH_3 stretching peak located in the 2865-2285 cm^{-1} range. The band width reduction and the presence of two resolved bands suggest a more ordered structure and underlines a modification of the hydrocarbon species by the electron beam irradiation. In particular, part of CH_x groups were damaged according to reactions (3), (4), (5) and (6) and bonded to the NW surface. After the treatment, a band located at about 520 cm^{-1} appeared and can be tentatively assigned to metal-carbon (M-C) stretching. This band, which is expected in the range 420-775 cm^{-1} for metal-alkyl and metal-alkenyl stretching,[56] supports the hypothesis that C atoms were bounded to Zn atoms on the surface of NW by the effect of energetic electron beam exposure. Instead, no substantial changes were observed in typical features of ZnO, corroborating the hypothesis that electron beam irradiation does not generate defects and do not affect the material crystal quality. Immediately after the O_2 plasma treatment, the initial situation was restored. As previously observed on the untreated sample, D and G carbon bands show again similar intensity with a I_D/I_G ratio close to 1 (Figure 7 b)). A general reduction of the CH_x stretching bands at 2800-3000 cm^{-1} was also observed after the plasma treatment, probably due to the removal of organic species from the surface and, more interestingly, the symmetric and asymmetric

stretching modes are again partially overlapped and not well resolved anymore (Figure 7 c)). Moreover, the Raman band located at about 520 cm^{-1} disappeared (Figure 7 a)), further supporting the assignment of this band to a C-Zn vibration. It can be then concluded that the bands separation induced by the bonding of organics on to the NW surface was removed by the plasma treatment.

The chemical differences on the surface of the e-beam irradiated area can be immediately visualized performing Raman maps across the exposed area, as shown in Figure 8 a). Here, it is evident that the surface modifications are not punctual observations but occurred all over the exposed area, confirming the selectivity of the electron beam treatment previously discussed. It is possible to observe in Figure 8 b) and c) an increase both in the intensity and the area of the G band, only in the irradiated area. This is a consequence of the degradation of the organic material and carbonization on the surface, as previously discussed. Furthermore, the M-C stretching band map showed higher intensity in the irradiated area, as can be noticed in Figure 8 d). This evidence corroborates the hypothesis that Zn-C bounds can be induced by the incident electron beam energy. As discussed before, Raman spectra presented two resolved peaks in the CH region in irradiated areas. In order to better visualize this in the Raman map in Figure 8 e), the colour map related to the ratio between the intensity of the peak located at 2925 cm^{-1} and the valley located at 2890 cm^{-1} is represented. In case of a high I_{2925}/I_{2890} ratio the minimum between the symmetric and the asymmetric mode bands is more pronounced and the two bands are more resolved. This clearly indicates that the CH band is splitted in two more resolved peaks in the e-beam irradiated area. The last colour map in Figure 8 f), built on the intensity ratio between the LO band (associated to ZnO defects, as previously discussed) and the E_2^{high} mode, confirms that electron beam irradiation does not generate defects in the material, since no significative

differences are noticed between the treated and not treated area. Moreover, Raman maps performed after the O_2 plasma treatment revealed that the surface modifications induced by e-beam irradiation were removed, supporting the reversibility of the electron beam treatment (see Supplementary Information S8).
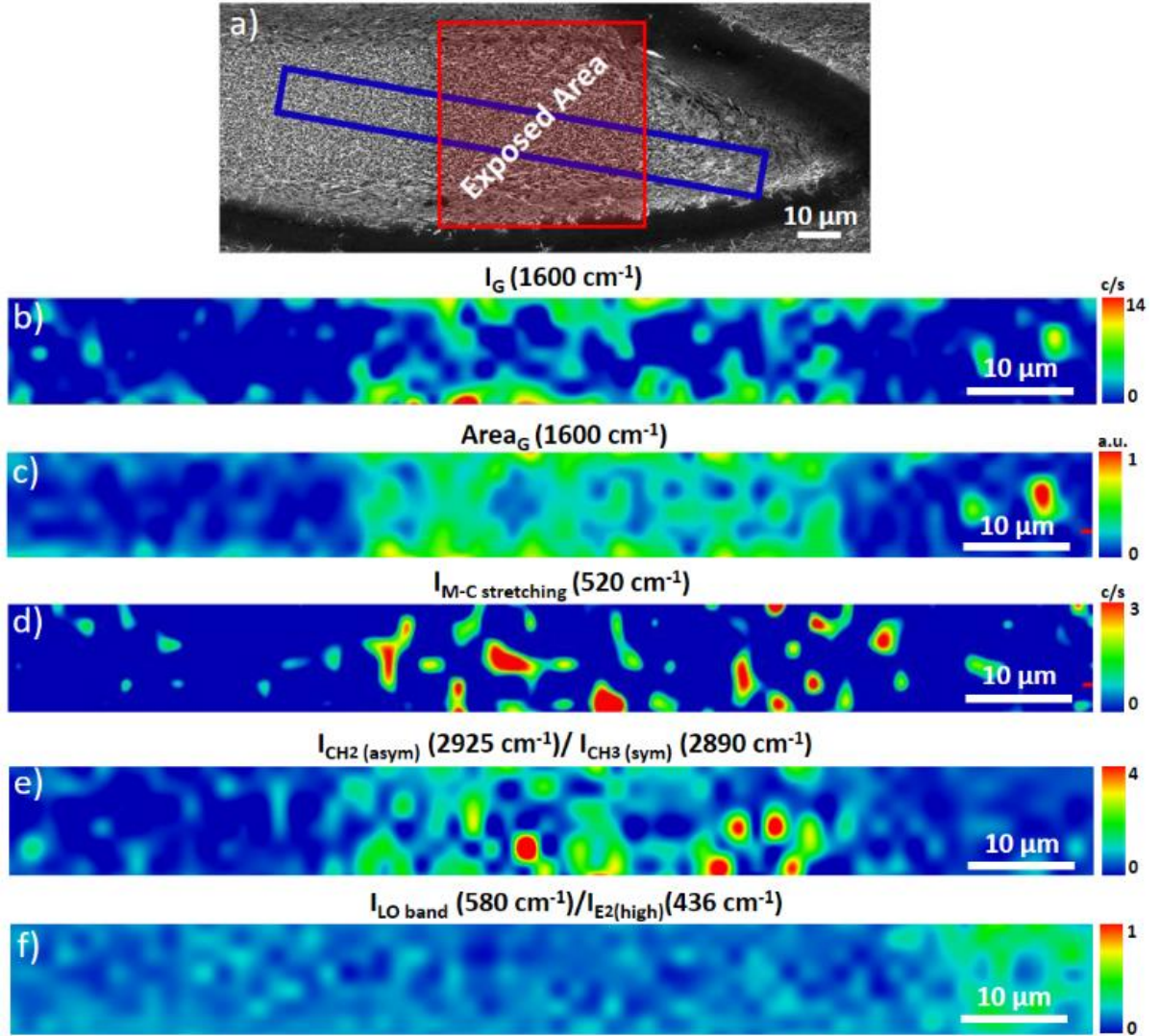
Figure 8. a) SEM image of vertically aligned ZnO NWs showing the electron beam irradiated area (red square) and the Raman map area (blue rectangle); Raman maps of G band (1600 cm-1) b) intensity and c) area; d) M-C stretching band intensity (520 cm-1); e) intensity ratio map between the intensity of the peak located at 2925 cm-1 and the peak located at 2890 cm-1 (CH region); f) LO band over E2high peak intensity ratio map.

The modifications of organic species on the surface after e-beam irradiation was also confirmed by FT-IR measurements. Relevant spectral differences before and after the electron treatment can be observed for symmetric and asymmetric C-H$_x$ stretching vibrations in the 2800-3000 cm^{-1} region, where FT-IR spectra were deconvoluted with Lorentzian/Gaussian peaks. In as grown samples, the peaks at 2853 cm^{-1} and 2925 cm^{-1} can be assigned to symmetric and asymmetric stretching modes of CH$_2$, respectively, while the bands at 2872 cm^{-1} and at 2961 cm^{-1} are due to symmetric and asymmetric stretching modes of CH$_3$ groups, respectively (Figure 9).[56] After electron beam irradiation the band intensities of C-H$_x$ stretching modes decreased as a consequence of the reduction of C-H$_x$ bonds (reactions (3)-(6)). In addition, as Figure 9 shows, a slight shift towards higher wavenumbers was observed for the most prominent bands in this
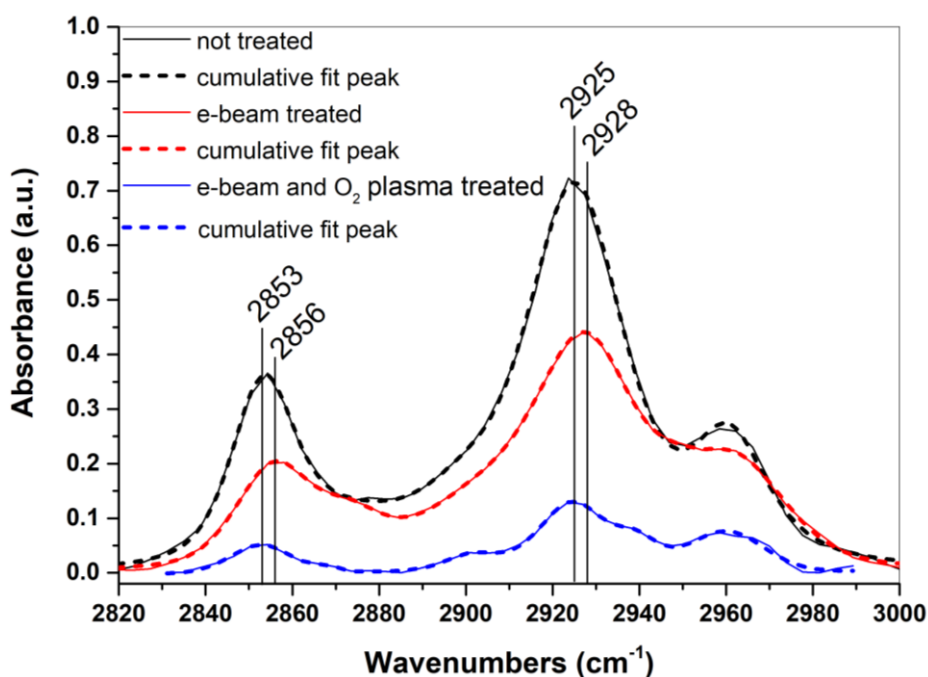

Figure 9. FT-IR measurements of the symmetric and asymmetric C-H stretching bands on the same area of vertically aligned ZnO NWs before treatments, after the e-beam treatment and after the O$_2$ plasma treatment. Continuous lines are raw data while fitted data are reported in dashed lines.

spectral region after electron beam irradiation. This shift is expected when C atoms are bounded to electronegative substituents, supporting the hypothesis that some radicals can be bounded to the NW surface. This shift was not clearly observed in Raman spectra, which is consistent to the low Raman activity of vibrational mode of dipolar bonds.[57] Moreover, the metal-methyl bonding reduces the C-H bond polarizability because of the directionality of the M-C bonding orbital and its consequent polarized character.[58] The intensity of $C-H_x$ stretching bands dramatically reduced immediately after O_2 plasma treatment as a consequence of the removal of organic species on the ZnO surface. As FTIR C-H region shows, the frequencies of the $C-H_x$ main bands returned to the position of the untreated sample, confirming the reversibility of the surface treatment (details of peak deconvolution, peak position and FWHM are presented in Supplementary Information S9).

To further elucidate the surface modification of ZnO and the role of $C-H_x$ compounds, the interaction of the electron beam treated ZnO surfaces and an organic polymer, poly-methyl methacrylate (PMMA), was investigated. PMMA diluted in anisole was spun on the substrate with ZnO NWs for 60 s at 2000 rpm, with a final thickness of ~ 320 nm. Subsequently, PMMA was annealed at a temperature of 165°C for 5 min in order to eliminate the solvents. Then, polymer was removed by an acetone bath (2 hours). In the opposite way respect to the corrosion process after water interaction, degradation of electron beam irradiated ZnO NWs was observed, as can be seen from Figure 10. In order to exclude that the degradation of irradiated ZnO NWs was due to the acetone used to remove PMMA, selected NWs were irradiated by electron beam and consequently exposed directly to acetone. In this case, electron beam treated NWs do not show any degradation even for long time exposure (details in Supplementary Information S10). As stated before, electron beam irradiation generated a CH-rich layer on the NW surface that possesses hydrophobic and oleophilic properties. This layer on the surface can easily interact

with organic molecules of PMMA, especially during the removal of solvents where long organic chains of PMMA can be bounded to C-H$_x$ species on the NW surface. In this case, the corrosion process of ZnO reasonably occurs when the polymer is removed by dissolving organic chains in acetone. Adopting the same strategy described before, degradation of electron beam-treated NWs after interaction with PMMA can be avoided by an O$_2$ plasma treatment (details in Supplementary Information S11). This evidence corroborated the hypothesis that the modification of the surface properties and reactivity of ZnO NWs was linked to electron beam
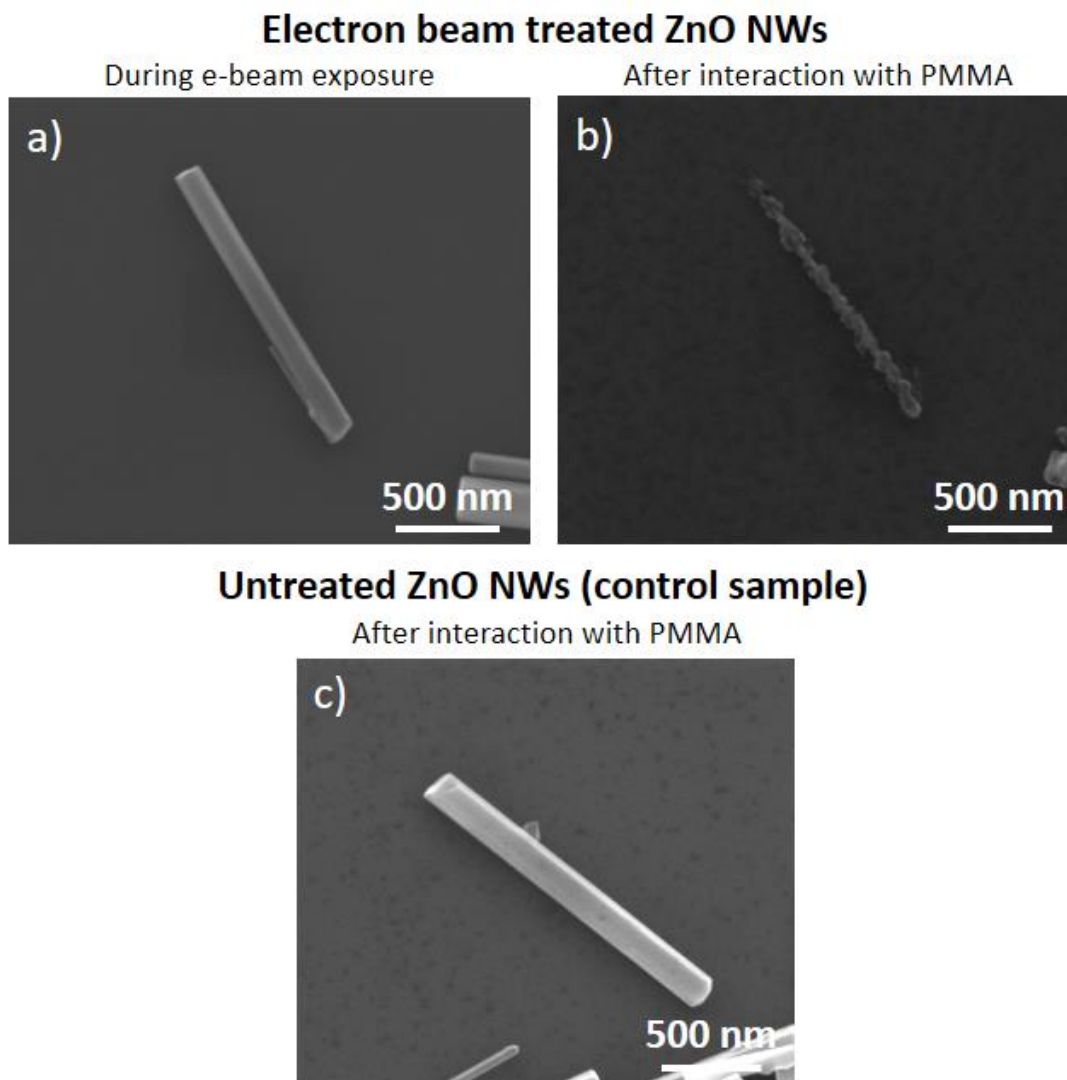
Figure 10. SEM image of the same ZnO NW on a SiO$_2$ substrate a) during e-beam exposure and b) after PMMA interaction; c) SEM image of an untreated ZnO NW after PMMA interaction (control sample).

induced organic groups on the NW surface. In the light of these observations, it is necessary to remark that particular attention must be paid during electron beam lithography processes involving ZnO NWs in order to avoid their degradation, since PMMA is commonly used as the resist material. Moreover, it is important to notice that this technique for tuning the wetting properties is particularly effective at the nanoscale because of electron beam irradiation over large areas requires long time of sample exposure. Since the contact angle measurements require large area (~ mm), a quantitative analysis of the wettability before and after treatment was not possible.

CONCLUSIONS

The anisotropic dissolution and corrosion process of ZnO NWs in water was analysed and an effective method for modifying the wetting properties of ZnO NWs by electron beam irradiation was investigated. A reversible switching of the surface properties from hydrophilic to hydrophobic was obtained, avoiding the ZnO NW dissolution. The modification of the surface wettability, deeply investigated by Raman and FT-IR spectroscopy, revealed that the surface free energy of the nanostructures was modified by electron beam irradiation as a consequence of the modification and decomposition of hydrocarbon species on the NW surface. This mechanism was further investigated by studying the interaction between electron beam treated ZnO NWs and an organic polymer (PMMA). Furthermore, it was observed that the initial hydrophilic situation can be restored using an O_2 plasma treatment, proving that this mechanism of surface modification is reversible. This approach can be used in controlling the dissolution and avoiding the corrosion of ZnO NWs and the same principle can be applied to other nanostructures and films. Thus, these observations can have an impact in a wide range of applications, from drug delivery to electronic device reliability.

AUTHOR INFORMATION

Corresponding Author

*Gianluca Milano, e-mail: gianluca.milano@polito.it

Author Contributions

G.M., L.D., S.P., and C.R designed the experiment. G.M. performed NW synthesis and characterization. G.M. and L.D. performed degradation studies, electron beam irradiation, oxygen plasma treatments and FE-SEM analyses. K.B. performed transmission electron microscopy. L.M. and A.M.G. performed spectroscopic measurements. G.M., S.P. and C.R. wrote the manuscript. All authors participated in the discussion of results and revision of the manuscript.

ASSOCIATED CONTENT

Supporting information

The Supporting Information is available free of charge on the ACS Publications website.

Additional high resolution XPS spectra of C 1s; additional high resolution XPS spectra of Zn $2_{p1/2}$; HRTEM images of ZnO NWs after water interaction; degradation of ZnO NWs dispersed on different substrates; selective tuning of the wetting properties of ZnO NWs; comparison of XPS spectra before and after electron beam irradiation; reversible tuning of wetting properties; Raman maps after O_2 plasma treatment; FT-IR spectra analysis; electron beam treated NWs and acetone interaction; effect of oxygen plasma treatment to avoid ZnO-PMMA interaction;

REFERENCES

(1)   Dasgupta, N. P.; Sun, J.; Liu, C.; Brittman, S.; Andrews, S. C.; Lim, J.; Gao, H.; Yan, R.; Yang, P. 25th Anniversary Article: Semiconductor Nanowires - Synthesis, Characterization, and Applications. *Adv. Mater.* **2014**, *26*, 2137–2183.

(2)   Yan, R.; Gargas, D.; Yang, P. Nanowire Photonics. *Nat. Photonics* **2009**, *3*, 569–576.

(3)   Sidiropoulos, T. P. H.; Röder, R.; Geburt, S.; Hess, O.; Maier, S. A.; Ronning, C.; Oulton, R. F. Ultrafast Plasmonic Nanowire Lasers near the Surface Plasmon Frequency. *Nat. Phys.* **2014**, *10*, 870–876.

(4)   Wen, B.; Sader, J. E.; Boland, J. J. Mechanical Properties of ZnO Nanowires. *Phys. Rev. Lett.* **2008**, *101*, 175502.

(5)   Chiu, S.-P.; Lin, Y.-H.; Lin, J.-J. Electrical Conduction Mechanisms in Natively Doped ZnO Nanowires. *Nanotechnology* **2009**, *20*, 15203.

(6)   Zhang, Y.; Ram, M. K.; Stefanakos, E. K.; Goswami, D. Y. Synthesis, Characterization, and Applications of ZnO Nanowires. *J. Nanomater.* **2012**, *2012*.

(7)   Djurišić, A. B.; Chen, X.; Leung, Y. H.; Man Ching Ng, A. ZnO Nanostructures: Growth, Properties and Applications. *J. Mater. Chem.* **2012**, *22*, 6526.

(8)   Chang, P.; Lu, J. G. ZnO Nanowire Field-Effect Transistors. *IEEE Trans. Electron Devices* **2008**, *55*, 2977–2987.

(9)   Milano, G.; Porro, S.; Ali, M. Y.; Bejtka, K.; Bianco, S.; Beccaria, F.; Chiolerio, A.; Pirri, C. F.; Ricciardi, C. Unravelling Resistive Switching Mechanism in ZnO NW Arrays: The Role of the Polycrystalline Base Layer. *J. Phys. Chem. C* **2018**, *122*, 866–874.

(10)　Porro, S.; Risplendi, F.; Cicero, G.; Bejtka, K.; Milano, G.; Rivolo, P.; Jasmin, A.; Chiolerio, A.; Pirri, C. F.; Ricciardi, C. Multiple Resistive Switching in Core–shell ZnO Nanowires Exhibiting Tunable Surface States. *J. Mater. Chem. C* **2017**, *5*, 10517–10523.

(11)　Laurenti, M.; Porro, S.; Pirri, C. F.; Ricciardi, C.; Chiolerio, A. Zinc Oxide Thin Films for Memristive Devices: A Review. *Crit. Rev. Solid State Mater. Sci.* **2017**, *42*, 153–172.

(12)　Wan, Q.; Li, Q. H.; Chen, Y. J.; Wang, T. H.; He, X. L.; Li, J. P.; Lin, C. L. Fabrication and Ethanol Sensing Characteristics of ZnO Nanowire Gas Sensors. *Appl. Phys. Lett.* **2004**, *84*, 3654–3656.

(13)　Stassi, S.; Chiadò, A.; Cauda, V.; Palmara, G.; Canavese, G.; Laurenti, M.; Ricciardi, C. Functionalized ZnO Nanowires for Microcantilever Biosensors with Enhanced Binding Capability. *c.* **2017**, *409*, 2615–2625.

(14)　Li, Z.; Yang, R.; Yu, M.; Bai, F.; Li, C.; Wang, Z. L. Cellular Level Biocompatibility and Biosafety of ZnO Nanowires. *J. Phys. Chem. C* **2008**, *112*, 20114–20117.

(15)　Zhang, Y.; Nayak, T. R.; Hong, H.; Cai, W. Biomedical Applications of Zinc Oxide Nanomaterials. *Curr. Mol. Med.* **2013**, *13*, 1633–1645.

(16)　Pan, Z.; Tao, J.; Zhu, Y.; Huang, J. F.; Parans Paranthaman, M. Spontaneous Growth of ZnCO3 Nanowires on ZnO Nanostructures in Normal Ambient Environment: Unstable ZnO Nanostructures. *Chem. Mater.* **2010**, *22*, 149–154.

(17)　Cimatu, K. A.; Mahurin, S. M.; Meyer, K. A.; Shaw, R. W. Nanoscale Chemical Imaging of Zinc Oxide Nanowire Corrosion. *J. Phys. Chem. C* **2012**, *116*, 10405–10414.

(18)　Kim, J.; Jeong, H. S.; Ahn, Y. H.; Lee, S.; Park, J. Y. Effects of Humidity on the Electrical Characteristics of ZnO Nanowire Devices. *Phys. Status Solidi Appl. Mater. Sci.* **2012**, *209*, 972–976.

(19) Chen, X.; Ng, A. M. C.; Djurišić, A. B.; Ling, C. C.; Chan, W. K. Hydrothermal Treatment of ZnO Nanostructures. *Thin Solid Films* **2012**, *520*, 2656–2662.

(20) Zhou, J.; Xu, N.; Wang, Z. L. Dissolving Behavior and Stability of ZnO Wires in Biofluids: A Study on Biodegradability and Biocompatibility of ZnO Nanostructures. *Adv. Mater.* **2006**, *18*, 2432–2435.

(21) Aronov, D.; Molotskii, M.; Rosenman, G. Electron-Induced Wettability Modification. *Phys. Rev. B* **2007**, *76*, 35437.

(22) Aronov, D.; Rosenman, G. Surface Energy Modification by Electron Beam. *Surf. Sci.* **2007**, *601*, 5042–5049.

(23) Aronov, D.; Molotskii, M.; Rosenman, G. Charge-Induced Wettability Modification. *Appl. Phys. Lett.* **2007**, *90*, 104104.

(24) Torchinsky, I.; Rosenman, G. Wettability Modification of Nanomaterials by Low-Energy Electron Flux. *Nanoscale Res. Lett.* **2009**, *4*, 1209–1217.

(25) Torchinsky, I.; Molotskii, M.; Rosenman, G. Induced Superhydrophobicity in ZnO Nanomaterial. *J. Nanoparticle Res.* **2010**, *12*, 2427–2433.

(26) Sabayev, V.; Aronov, D.; Oster, L.; Rosenman, G. Electron-Induced Surface Reactivity Modification in Zinc Oxide-Based Thin Films. *Appl. Phys. Lett.* **2008**, *93*, 144104.

(27) Rocchia, M.; Borini, S.; Rossi, A. M.; Boarino, L.; Amato, G. Submicrometer Functionalization of Porous Silicon by Electron Beam Lithography. *Adv. Mater.* **2003**, *15*, 1465–1469.

(28) Djenizian, T.; Salhi, B.; Boukherroub, R.; Schmuki, P. Bulk Micromachining of Silicon Using Electron-Beam-Induced Carbonaceous Nanomasking. *Nanotechnology* **2006**, *17*, 5363–5366.

(29)　Borini, S.; Amato, G.; Rocchia, M.; Boarino, L.; Rossi, A. M. Electron-Beam Irradiation of Porous Silicon: Application to Micromachining. *J. Appl. Phys.* **2003**, *93*, 4439–4441.

(30)　Imbraguglio, D.; Giovannozzi, A. M.; Nastro, A.; Rossi, A. M. Submicron Machining and Biomolecule Immobilization on Porous Silicon by Electron Beam. *Nanoscale Res. Lett.* **2012**, *7*, 1–8.

(31)　Egerton, R. F.; Li, P.; Malac, M. Radiation Damage in the TEM and SEM. *Micron* **2004**, *35*, 399–409.

(32)　Podrezova, L. V; Porro, S.; Cauda, V.; Fontana, M.; Cicero, G. Comparison between ZnO Nanowires Grown by Chemical Vapor Deposition and Hydrothermal Synthesis. *Appl. Phys. a-Materials Sci. Process.* **2013**, *113*, 623–632.

(33)　David, C. A.; Galceran, J.; Rey-Castro, C.; Puy, J.; Companys, E.; Salvador, J.; Monné, J.; Wallace, R.; Vakourov, A. Dissolution Kinetics and Solubility of ZnO Nanoparticles Followed by AGNES. *J. Phys. Chem. C* **2012**, *116*, 11758–11767.

(34)　Jiang, C.; Hsu-Kim, H. Direct in Situ Measurement of Dissolved Zinc in the Presence of Zinc Oxide Nanoparticles Using Anodic Stripping Voltammetry. *Environ. Sci. Process. Impacts* **2014**, *16*, 2536–2544.

(35)　Yadav, K.; Mehta, B. R.; Lakshmi, K. V.; Bhattacharya, S.; Singh, J. P. Tuning the Wettability of Indium Oxide Nanowires from Superhydrophobic to Nearly Superhydrophilic: Effect of Oxygen-Related Defects. *J. Phys. Chem. C* **2015**, *119*, 16026–16032.

(36)　Yadav, K.; Mehta, B. R.; Bhattacharya, S.; Singh, J. P. A Fast and Effective Approach for Reversible Wetting-Dewetting Transitions on ZnO Nanowires. *Sci. Rep.* **2016**, *6*, 35073.

(37)　Al-Sabahi, J.; Bora, T.; Al-Abri, M.; Dutta, J. Controlled Defects of Zinc Oxide Nanorods

for Efficient Visible Light Photocatalytic Degradation of Phenol. *Materials (Basel).* **2016**, *9*, 238.

(38) Jeong, Y.; Bae, C.; Kim, D.; Song, K.; Woo, K.; Shin, H.; Cao, G.; Moon, J. Bias-Stress-Stable Solution-Processed Oxide Thin Film Transistors. *ACS Appl. Mater. Interfaces* **2010**, *2*, 611–615.

(39) Jung, Y.; Yang, W.; Koo, C. Y.; Song, K.; Moon, J. High Performance and High Stability Low Temperature Aqueous Solution-Derived Li–Zr Co-Doped ZnO Thin Film Transistors. *J. Mater. Chem.* **2012**, *22*, 5390.

(40) Zhang, B.; Zhou, H. B.; Han, E. H.; Ke, W. Effects of a Small Addition of Mn on the Corrosion Behaviour of Zn in a Mixed Solution. *Electrochim. Acta* **2009**, *54*, 6598–6608.

(41) Zheng, J. H.; Jiang, Q.; Lian, J. S. Synthesis and Optical Properties of Flower-like ZnO Nanorods by Thermal Evaporation Method. *Appl. Surf. Sci.* **2011**, *257*, 5083–5087.

(42) Feng, X.; Feng, L.; Jin, M.; Zhai, J.; Jiang, L.; Zhu, D. Reversible Super-Hydrophobicity to Super-Hydrophilicity Transition of Aligned ZnO Nanorod Films. *J. Am. Chem. Soc.* **2004**, *126*, 62–63.

(43) Ali, M.; Winterer, M. ZnO Nanocrystals: Surprisingly "Alive." *Chem. Mater.* **2010**, *22*, 85–91.

(44) Qi, J.; Zhang, K.; Ji, Z.; Xu, M.; Wang, Z.; Zhang, Y. Dissolving Behavior and Electrical Properties of ZnO Wire in HCl Solution. *RSC Adv.* **2015**, *5*, 44563–44566.

(45) Gunko, V. M.; Turov, V. V; Zarko, V. I.; Voronin, E. F.; Tischenko, V. A.; Dudnik, V. V; Pakhlov, E. M.; Chuiko, A. A. Active Site Nature of Pyrogenic Alumina/silica and Water Bound to Surfaces. *Langmuir* **1997**, *13*, 1529–1544.

(46) Yoshiie, T.; Iwanaga, H.; Shibata, N.; Ichihara, M.; Takeuchi, S. Orientation Dependence

of Electron–irradiation Damage in Zinc Oxide. *Philos. Mag. A Phys. Condens. Matter, Struct. Defects Mech. Prop.* **1979**, *40*, 297–301.

(47)   Seshadri, K.; Froyd, K.; Parikh, A. N.; Allara, D. L.; Park, U. V; Pennsyl, V.; Lercel, M. J.; Craighead, H. G. Electron-Beam-Induced Damage in Self-Assembled Monolayers. **1996**, *3654*, 15900–15909.

(48)   Botman, A.; Mulders, J. J. L.; Hagen, C. W. Creating Pure Nanostructures from Electron-Beam-Induced Deposition Using Purification Techniques: A Technology Perspective. *Nanotechnology* **2009**, *20*, 372001.

(49)   Djenizian, T.; Santinacci, L.; Schmuki, P. Electron Beam-Induced Carbon Masking for Electrodeposition on Semiconductor Surfaces. *Appl. Phys. Lett.* **2001**, *78*, 2940–2942.

(50)   Cuscó, R.; Alarcón-Lladó, E.; Ibáñez, J.; Artús, L.; Jiménez, J.; Wang, B.; Callahan, M. Temperature Dependence of Raman Scattering in ZnO. *Phys. Rev. B* **2007**, *75*, 165202.

(51)   Yang, L. li; Yang, J. hai; Wang, D. dan; Zhang, Y. jun; Wang, Y. xin; Liu, H. lian; Fan, H. gang; Lang, J. hui. Photoluminescence and Raman Analysis of ZnO Nanowires Deposited on Si(1 0 0) via Vapor-Liquid-Solid Process. *Phys. E Low-Dimensional Syst. Nanostructures* **2008**, *40*, 920–923.

(52)   Manjón, F. J.; Marí, B.; Serrano, J.; Romero, A. H. Silent Raman Modes in Zinc Oxide and Related Nitrides. *J. Appl. Phys.* **2005**, *97*, 1–4.

(53)   Tuinstra, F.; Koenig, L. Raman Spectrum of Graphite. *J. Chem. Phys.* **1970**, *53*, 1126–1130.

(54)   Snyder, R. G.; Scherer, J. R. Band Structure in the C–H Stretching Region of the Raman Spectrum of the Extended Polymethylene Chain: Influence of Fermi Resonance. *J. Chem. Phys.* **1979**, *71*, 3221.

(55)   Gong, Y. T.; Li, B. H.; Pei, T.; Lin, C. H.; Lee, S. Raman Investigation on Carbonization Process of Metal-Organic Frameworks. *J. Raman Spectrosc.* **2016**, *47*, 1271–1275.

(56)   Socrates, G. *Infrared and Raman Characteristic Group Frequencies: Tables and Charts*; John Wiley & Sons: Chichester, 2001.

(57)   Halford, R. S. Motions of Molecules in Condensed Systems: I. Selection Rules, Relative Intensities, and Orientation Effects for Raman and Infra-Red Spectra. *J. Chem. Phys.* **1946**, *14*, 8–15.

(58)   Schilling, J. B.; Goddard, W. A.; Beauchamp, J. L. Theoretical Studies of Transition-Metal Methyl Ions, Mch3+(m = Sc, Cr, Mn, Zn, Y, Mo, Tc, Pd, Cd). *J. Am. Chem. Soc.* **1987**, *109*, 5573–5580.

Hydrophilic ZnO NWs

Electron beam irradiation
Hydrocarbons decomposition

O₂ plasma
Removal of organic species

Hydrophobic ZnO NWs

Anisotropic dissolution in H₂O

No dissolution in H₂O